Reversible Discrete-to-Extended Metal–Organic Polyhedra Transformation by Sulfonic Acid Surface Functionalization

Javier Troyano,* Satoshi Horike and Shuhei Furukawa*

Institute for Integrated Cell-Material Sciences (WPI-iCeMS), Kyoto University, iCeMS Research Building, Yoshida, Sakyo-ku, Kyoto 606-8501, Japan

Department of Synthetic Chemistry and Biological Chemistry, Graduate School of Engineering, Kyoto University, Katsura, Nishikyo-ku, Kyoto 615-8510, Japan

Inorganic Chemistry Department, Autonomous University of Madrid, Madrid 28049, Spain

KEYWORDS Molecules, Functionalization, Organic acids, Water, Polymerization, Metal organic frameworks

ABSTRACT: Metal–organic polyhedra (MOPs) are molecular porous units in which desired functionalities can be installed with precise geometrical and compositional control. By combing two complementary chemical moieties, such as sulfonic acid group and Rh(II)-carboxylate paddlewheel, we synthesized a robust water-soluble cuboctahedral MOP with excellent features in both solution and solid state. Herein, we demonstrate that the superior chemical stability of the Rh_2 unit and the elevated number of functional groups on the surface (24 per cage) result in a porous cage with high solubility and stability in water, including acidic, neutral and basic pH conditions. We also prove that the sulfonic acid-rich form of the cage can be isolated through post-synthetic acid treatment. This transformation involves an improved gas uptake capacity, and the capability to reversibly assemble the cages into a 3D metal–organic framework (MOF) structure. Likewise, this sulfonic acid functionalization provides both MOP and MOF solids with high proton conductivities ($> 10^{-3}$ S cm^{-1}), comparable to previously reported high conducting metal-organic materials. The influence of the MOP-to-MOF processing in the gas adsorption capacity indicates this structural transformation can provide materials with higher and more controllable porous properties. These results illustrate the high potential of acidic MOPs as more flexible porous building units in terms of processability, structural complexity and tunability of the properties.

INTRODUCTION

The assembly of metal ions and organic ligands provides access to two main types of ordered porous materials: metal–organic frameworks (MOFs), in which direct assembly results in extended architectures; and metal-organic polyhedra (MOPs) or metal–organic cages (MOCs), where the assembly generates a molecular complex that encloses a geometrically defined inner cavity.[1] Conceptually, a MOP can be regarded as the zero-dimensional analogue of a MOF;[2] thus, both can be designed to display well-defined porous structures and incorporate specific chemical functions that lead to targeted features. However, compared to extended MOFs, the discrete nature of MOPs implies a substantial difference in their physicochemical properties and consequently, in their potential uses and applications.[3-5] Foremost, MOPs can be dissolved while maintaining their porous structure, facilitating their practical use in solution. Further, their molecular character enables the precise adjustment of their geometry,[6] composition,[7] and external surface functionalization.[8] The latter aspect is particularly relevant as it allows to adjust the hydrophilic/hydrophobic nature of the cages,[9] modify their solubility in different solvents,[10] improve their stability,[11] tune their acid/base properties,[12] and favor specific interactions with (bio)chemical systems.[13]

Apart from fostering their use in solution, the control over MOPs surface functionalization also makes it possible to regulate their assembly in the solid state. Indeed, thanks to their well-defined geometry and the stoichiometric control over the external reactive functional groups, MOPs can be used as building blocks for constructing extended MOFs.[14,15] This strategy provides a more practical and flexible scenario. On one hand, MOPs can be designed as individual porous units for achieving novel supramolecular arrangements following a bottom-up modular approach.[16,17] On the other hand, resulting MOFs can be disassembled into discrete MOP molecules retaining their functionality once dissolved, making it possible to use them in solution or be further processed as MOP/MOF solid on demand. Despite these beneficial aspects, such "MOP-to-MOF" transformations have been scarcely investigated. Reported examples followed two main approaches: i) exploiting potential open metal sites by coordination of additional linkers,[18,19] and ii) using external functional groups to connect them through condensation with reactive organic molecules,[20] or by coordination with additional metal ions.[21,22]

Alternatively, a more attractive possibility relies on the formation of coordination bonds between complementary donor and acceptor groups in the cage. This approach offers a simpler route, which does not involve additional components and facilitates the reversibility of the MOP-to-MOF transformation.

This coordination-driven self-polymerization was first demonstrated by Zaworotko *et al*., showing the formation of a 1-dimensional network based on inter-cage coordination bonds between donor -OMe group and acceptor Cu_2 units, both present in the methoxy-functionalized Cu(II) cuboctahedron, $[Cu_{24}(OMe\text{-}bdc)_{24}]$, (OMe-bdc = 5-methoxy-1,3-benzenedicarboxylate).[22] Later, Ma *et al*. used the hydroxy-functionalized analogue, $[Cu_{24}(OH\text{-}bdc)_{24}]$, (OH-bdc = 5-hydroxy-1,3-benzenedicarboxylate) for the construction of 2- and 3-dimensional frameworks *via* similar reciprocal inter-cage bonding between -OH group and Cu.[23,24] However, the reversibility of the MOP-to-MOF process is yet to be reported.

Despite the simplicity of this strategy, there are several limitations that need to be tackled to achieve such transformation. One important obstacle is related to the incorporation of chemical groups with coordinating ability (e.g. -COOH, $-NH_2$), which typically lead to undesired extended coordination networks during MOP synthesis. An effective strategy to overcome this issue is to use specific protecting groups, however it requires additional protection and deprotection steps.[10] Likewise, many MOPs are built-up by coordinatively saturated metallic nodes (e.g. $[Cp_3Zr_3O(OH)_3]$, $[Pd(pyridyl)_4]$, $[Pt(pyridyl)_4]$), which hinders their further extension. Finally, another impediment is the low stability of many MOPs under self-polymerization conditions (e.g. temperature, pH).

In this work, we introduced the versatile sulfonic acid moiety ($-SO_3H$) in the external surface of robust Rh(II) paddlewheel-based cuboctahedron. As a consequence of such functionalization, the resulting cage, $[Rh_{24}(SO_3H\text{-}bdc)_{24-x}(SO_3\text{-}bdc)_x]^{-x}$ (**SO_3H/SO_3-RhMOP**; where SO_3H-bdc = isophthalate-5-sulfonic acid and SO_3-bdc = 5-sulfo-1,3-benzenedicarboxylate), was highly soluble in water at both acid and basic media. In this case, the use of "weak" coordinating $-SO_3H$ group prevented the formation of extended networks during MOP construction. Further, this cage could be post-synthetically modified by acid treatment to display different acidic properties (Figure 1). In solution, cage solubility in polar organic solvents could be attained by increasing the SO_3H/SO_3 ratio. In addition, acid treated MOP cages were reversibly cross-linked through coordination of SO_3H groups to available Rh(II) paddlewheel axial positions, resulting in the formation of $[Rh_3(SO_3H\text{-}bdc)_3(H_2O)_2]_n$ (**SO_3H-RhMOF**) MOF crystals. The effect of the self-polymerization of MOP cages on the adsorption properties was examined in terms of intrinsic (inner cavity) and extrinsic (cage arrangement) porosity. In addition, thanks to the well-known ability of sulfonic acid groups for proton conduction, resulting compounds presented high proton conductivity (up to ~10^{-2} S cm^{-1}) comparable to the highest values previously reported for MOPs.

RESULTS AND DISCUSSION

Design, synthesis, and acidic properties of SO_3H/SO_3-RhMOP. Previous examples of MOPs with pending sulfonic groups have been prepared by combining linkers containing other groups with stronger coordination ability (i.e. imines, carboxylates), and either hard (i.e.

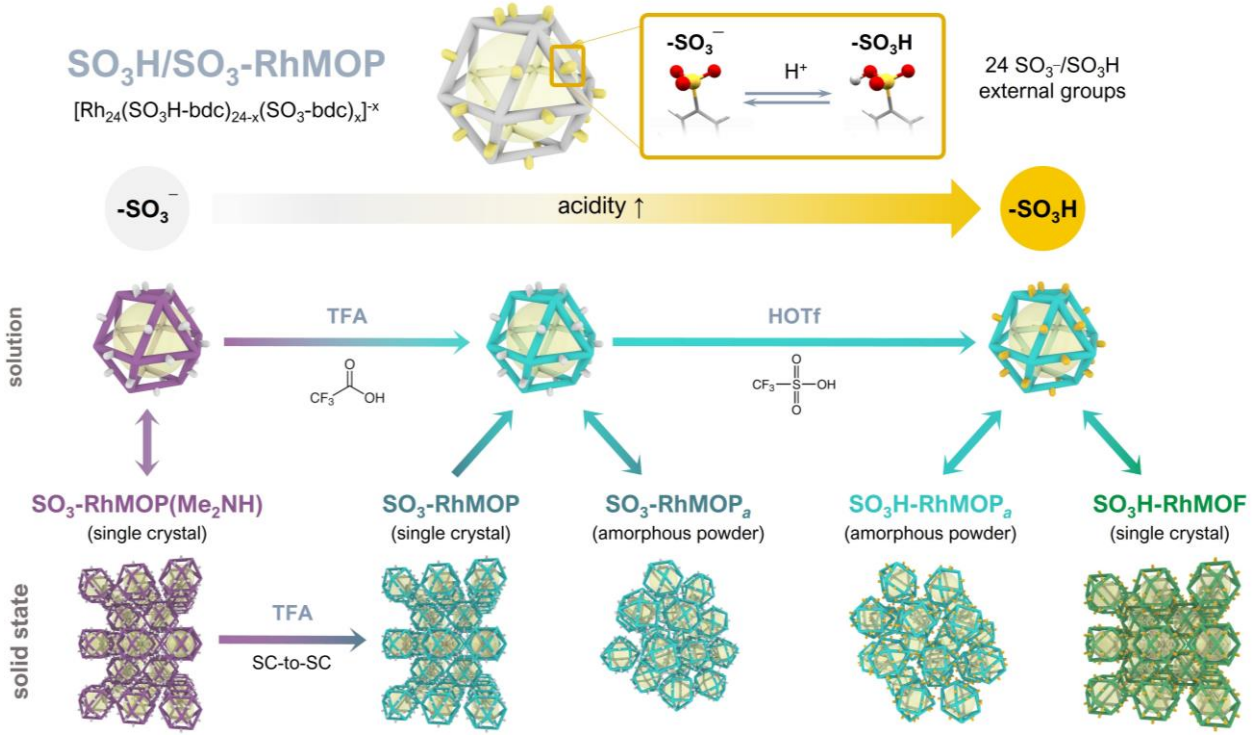

Figure 1. Schematic overview of transformations involving **SO_3H/SO_3-RhMOP** in both solution and solid state described in this work.

Zr(IV))[25] or soft (e.g. Fe(II), Zn(II)) metal ions with saturated coordination spheres.[26,27] Consequently, sulfonic groups are prevented to coordinate during cage synthesis, but at the cost of hindering the further self-polymerization through sulfonic group coordination. The case of cuboctahedral Cu(II) MOP with external sulfonic groups constitutes an exception, since this cage presents both open metal sites and external sulfonic groups.[28] However, the low stability of Cu-carboxylate towards moisture and acids limits the exploitation of such functionalization.

In this work, we chose Rh(II) paddlewheel unit with 5-sulfo-1,3-benzenedicarboxylic acid (SO_3H-bdc) to construct a cuboctahedron MOP. This type of cage offers a high density of functional groups on the surface, which is expected to enhance the acidic capacity and proton conduction. Likewise, the higher number of potential connection points provides more flexibility upon network formation. The softer character of Rh(II) ions and the twelve available open metal sites on the surface allow the extension *via* coordination bonds with soft sulfonic groups. In addition, the $[Rh_2(COO)_4]$ unit offers superior stability, enabling further post-synthetic modification and use.

The reaction of $[Rh_2(OAc)_4]$ with SO_3H-bdc in DMA/water solvent mixture at 120 °C resulted in the formation of purple single crystals of $[Rh_{24}(SO_3\text{-bdc})_{24}(Me_2NH)_{12}(H_2O)_4(DMA)_8]^{24-}$ (**SO_3-RhMOP(Me_2NH)**, where Me_2NH = dimethylamine and DMA = *N*,*N*-dimethylacetamide). Single crystal X-ray diffraction (SC-XRD) analysis revealed that **SO_3-RhMOP(Me_2NH)** crystallizes in the tetragonal space group $I4/m$, containing two cages in the unit cell (Table S1). The molecular structure of **SO_3-RhMOP(Me_2NH)** consists of twelve Rh_2 paddlewheel nodes connected through twenty-four 5-sulfo-1,3-benzenedicarboxylate ligands to form a cuboctahedral architecture (Figure 2a). The size of the cage, defined by the average distance between centroids of the O atoms in -SO_3 groups of the opposing dicarboxylate ligands, was estimated in *ca*. 2.9 nm. Likewise, the pore size of **SO_3-RhMOP(Me_2NH)**, defined by the average distance between the opposing internal Rh atoms, was found to be *ca*. 1.6 nm. In **SO_3-RhMOP(Me_2NH)** the external axial positions of Rh2 units are occupied by coordinated DMA and water molecules, while all internal positions are occupied by Me_2NH molecules. In the crystal packing of **SO_3-RhMOP(Me_2NH)**, each cage is surrounded by eight equivalent neighboring cages located at the vertices of a tetragonal prism (Figure 2b). This array involves the alignment of the cages along the [001] direction, resulting in the formation of solvent accessible channels (Figure 2c).

During the synthesis of **SO_3-RhMOP(Me_2NH)**, we found that the addition of water was essential to obtain the crystals. All the screened reactions in DMA resulted in amorphous powders (Figures S1 and S2). This effect can be attributed to the hydrophilic nature of the cage, which makes the addition of water to increase its solubility, favoring crystallization. Besides, the presence of water also involved the hydrolysis of DMA solvent, leading to the formation of Me_2NH molecules.[29] Such *in-situ* generated Me_2NH molecules are able to coordinate to internal axial positions of Rh_2 dimers causing the purple color of **SO_3-RhMOP(Me_2NH)** crystals.[30] This was confirmed by SC-XRD and ^{1}H NMR (Figure S3). The removal of coordinated dimethylamine was easily performed by acid treatment of **SO_3-RhMOP(Me_2NH)** crystals with trifluoroacetic acid (TFA), leading to turquoise crystals of $[Rh_{24}(SO_3\text{-bdc})_{24}(H_2O)_{16}(DMA)_8]^{-24}$ (**SO_3-RhMOP**) in a single-crystal-to-single-crystal (SC-to-SC) fashion (Figures 1d, S2, S4 and Video S1). **SO_3-RhMOP** presents an analogous crystal structure to that found in **SO_3-RhMOP(Me_2NH)**, but in

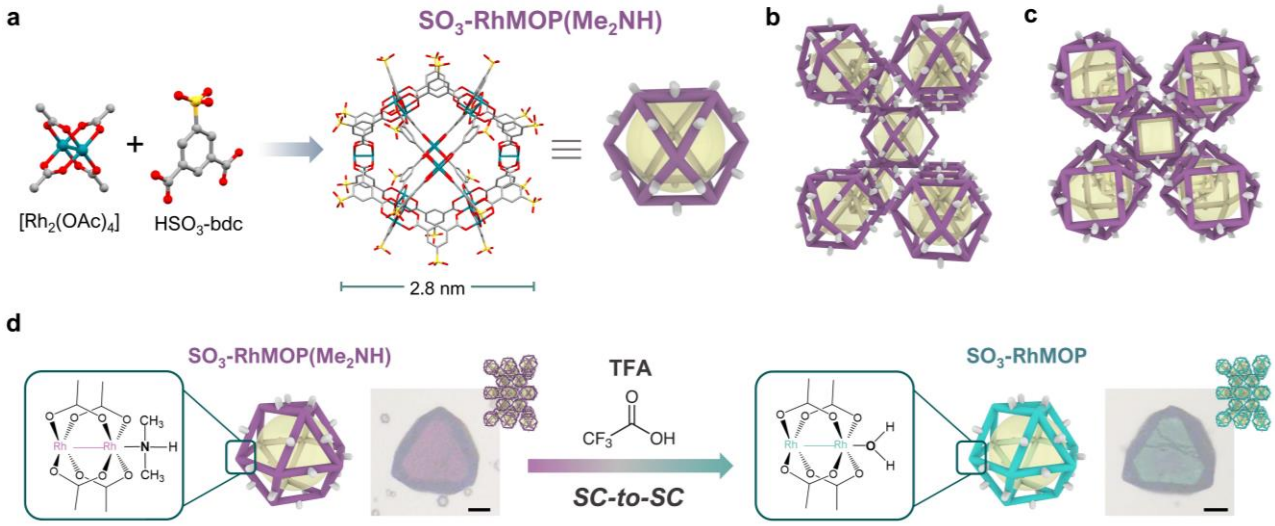

Figure 2. a) Schematic representation of the synthesis of **SO_3-RhMOP(Me_2NH)** from its building blocks. b) View of the molecular packing in **SO_3-RhMOP(Me_2NH)** crystals. c) View of the projection of the crystal structure of **SO_3-RhMOP(Me_2NH)** along the *c* axis, showing the alignment of the cage pores. d) SC-to-SC conversion of **SO_3-RhMOP(Me_2NH)** into **SO_3-RhMOP** as a consequence of the substitution of internally coordinated Me_2NH molecules by water upon treatment with TFA (scale bar = 100 μm).

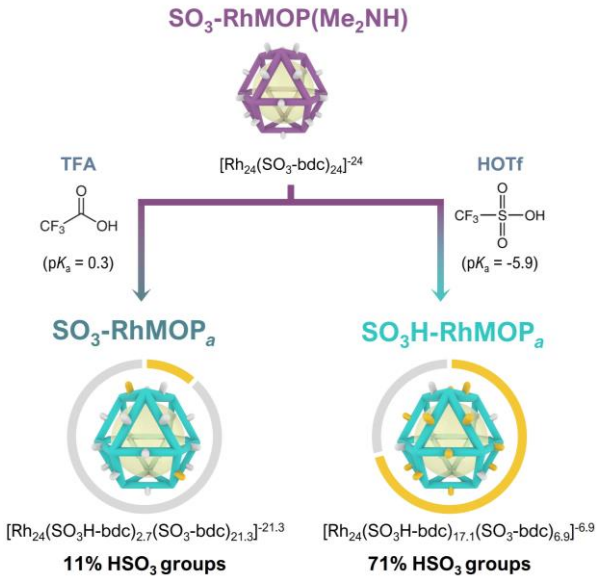

Figure 3. Schematic representation of the preparation of **SO_3-RhMOP$_a$** and **SO_3H-RhMOP$_a$** by treatment of **SO_3-RhMOP(Me_2NH)** with TFA and HOTf, respectively, showing the different protonation degree.

SO_3-RhMOP dimethylamine molecules at internal axial positions are replaced by water molecules, leading to turquoise color (Figures S5 and S6).[30] Such structural analogy between both structures helps to explain the observed SC-to-SC transformation (Table S2).

We synthesized bulk **SO_3-RhMOP$_a$** solid by first dissolving as-made **SO_3-RhMOP(Me_2NH)** crystals in MeOH, adding TFA to the resulting solution and then precipitating with diethyl ether to give a turquoise amorphous powder. Thanks to the hydrophilic nature of -SO_3^- group, **SO_3-RhMOP$_a$** was found to be highly soluble in water and methanol, but insoluble in other organic solvents. We attributed this behavior to the formation of an ionic pair between anionic $[Rh_{24}(SO_3\text{-bdc})_{24}]^{-24}$ cage and cationic dimethyl ammonium, $[Me_2NH_2]^+$, generated upon acid treatment. This was confirmed by ^{1}H NMR studies (Figure S7) and elemental analysis (Table S2), showing an approximate SO_3-bdc:$[Me_2NH_2]^+$ ratio of 1:1. The number of -SO_3H groups was estimated in ~2.7 per cage by titration with aqueous NaOH (Figures 3 and S8), confirming the anionic character of the cage. The prevalence of the deprotonated form of the cage, even after TFA treatment, was ascribed to the higher acidity of arylsulfonic acids (e.g. SO_3H-Ph, pK_a = -2.8)[31] compared to TFA (pK_a = 0.3). Correspondingly, we used stronger triflic acid (HOTf, pK_a = -5.9)[31] to produce the sulfonic acid functionalized cage (Figure 3). **SO_3-RhMOP(Me_2NH)** was dissolved in methanol, treated with HOTf and precipitated with diethyl ether. After washing, turquoise amorphous bulk powder **SO_3H-RhMOP$_a$** was obtained (Figure S9). HOTf treated **SO_3H-RhMOP$_a$** was found to be soluble in water and methanol, but also in other polar organic solvents, such as ethanol, ethylene glycol, DMF or DMSO (Figure 4a). Following this methodology, the number of -SO_3H groups per cage was successfully increased from 2.7 (11%) to 17.1 (71%) (Figure S10), which correlates with the improved solubility of **SO_3H-RhMOP$_a$** in organic solvents. Further, a comparison of elemental analysis data for vacuum-heated **SO_3-RhMOP$_a$** and **SO_3H-RhMOP$_a$** samples showed a near-total removal of the nitrogen content in **SO_3H-RhMOP$_a$**, with N/S ratio values of 1.22 and 0.14, respectively (Table S3). Likewise, the different chemical composition between **SO_3-RhMOP$_a$** and **SO_3H-RhMOP$_a$** was confirmed by thermogravimetric analysis (TGA) (Figure S11).

Compared to other previously reported water-soluble cages, the combination of $[Rh_2(CO_2)_4]$ metal cluster with SO_3H-bdc ligand provides **SO_3H-RhMOP$_a$** with valuable properties in solution. First, the use of Rh confers the material an excellent chemical stability, preventing its decomposition in water, as observed for analogous Cu(II) derivatives.[28,32] In addition, thanks to the high acidity of the sulfonic acid, **SO_3H-RhMOP$_a$** can be dissolved in highly acid (pH = 0.5) and basic (pH = 11) aqueous media, showing no degradation over time (i.e. one month), as indicated by UV-vis measurements (Figures 4b and 4c). This behavior differs from previously reported Rh-based cages with terminal hydrophilic groups, such as -OH or –COOH, which

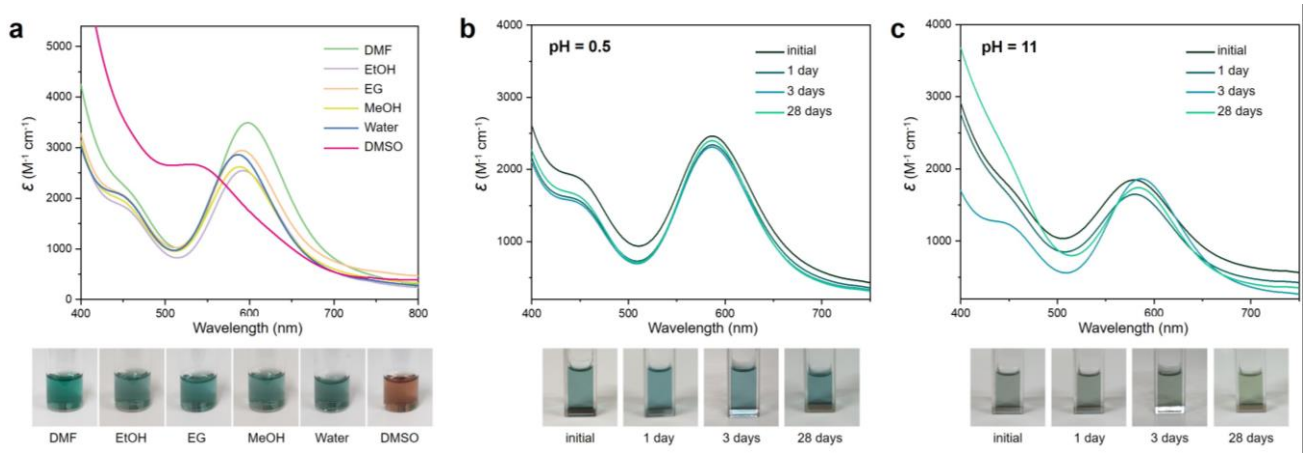

Figure 4. UV-vis spectra (top) and photographs (bottom) of **SO_3H-RhMOP$_a$** solutions in different solvents (a) and in water at pH = 0.5 (b) and pH = 11 (c) over time.

can only be dissolved in basic aqueous media (pH > 8) due to their weaker acidity.[10]

Self-polymerization of SO_3H-RhMOP into SO_3H-RhMOF. A very attractive aspect of **SO_3H-RhMOP** cage is the presence of both open metal sites and potential coordinating sulfonic acid groups in its structure. This feature prompted us to explore the possibility of assembling **SO_3H-RhMOP** into an extended coordination network. In our case, for the formation of extended networks *via* coordination of sulfonic acids, two important aspects of their chemistry were considered: i) their weak coordination ability and ii) their high acidity. Traditionally, sulfonic acids has been considered as poor ligands, since reactions with transition metals ions usually result in the formation of ionic pairs between sulfonate and solvated metal ions.[33-36] Thus, the polymerization processes of **SO_3H-RhMOP** is expected to be hindered by the competition between solvent and weakly coordinating sulfonic groups. Further, because of its high acidity, sulfonic groups can easily deprotonate in solution to form negatively charged $^{-}SO_3^{-}$ functionalized cages. This scenario results unpropitious for polymerization reaction for two reasons. First, it involves the electrostatic repulsion between the cages, preventing them to react.[37] Second, the coordination of negatively charged $-SO_3^{-}$ group to neutral Rh_2 dimer is adverse because of charge balance requirements.

With these considerations in mind, we investigated the self-polymerization of **SO_3H-RhMOP** in water in the presence of HOTf (Figure 5a). We found that after almost total evaporation of a solution of **SO_3H-RhMOP$_a$** in water:HOTf (80:1, v/v) solvent mixture at 80 °C, green crystals of **SO_3H-RhMOF** were obtained (Figures S12 and S13). SC-XRD analysis revealed that under these conditions, **SO_3H-RhMOP** cages assemble into a 3D MOF architecture, **SO_3H-RhMOF** (Table S4). The crystal structure of **SO_3H-RhMOF** is very similar to **SO_3-RhMOP**, with space group *I*4/*m* and two MOP molecules per unit cell. However, in **SO_3H-RhMOF** each cage is coordinatively connected to the eight equivalent neighboring cages situated at the vertices of a tetragonal prism. This linkage is based on the coordination of one oxygen atom of one $-SO_3H$ group of the central cage to the external axial position of an Rh_2 dimer of a neighboring cage (Figure 5b). Reciprocally, each one of these cages coordinates in the same fashion to one of the eight geometrically accessible Rh_2 units of the central cage. Consequently, in **SO_3H-RhMOF** each cage presents sixteen non-coordinated sulfonic groups and four coplanar Rh_2 dimers with non-connected external sites, which are occupied by coordinated water molecules (Figure S14). The Rh-O(sulfonic) bond length is 2.325 Å, which falls within the range of typical M–O bond of aryl sulfonate complexes (Figures S15 and S16) and previously reported Rh(II)-based MOPs with O-donor ligands (2.224-2.383 Å).[38-40] Note here that while the coordination of triflate anion (OTf^{-}) to Rh(I) and Rh(III) in organometallic complexes is well-known,[41,42] the OTf^{-} coordination of Rh(II) is extremely rare with only one previous precedent.[43] To our knowledge, **SO_3H-RhMOF** represents the first example of an 8-connected (8-c) network based on the crystalline assembly of MOPs. Previous examples based on OH-functionalized Cu MOP (*vide supra*) resulted into 4-c, 6-c and (4,6)-c networks, where the role of coordinated solvent molecules determines the

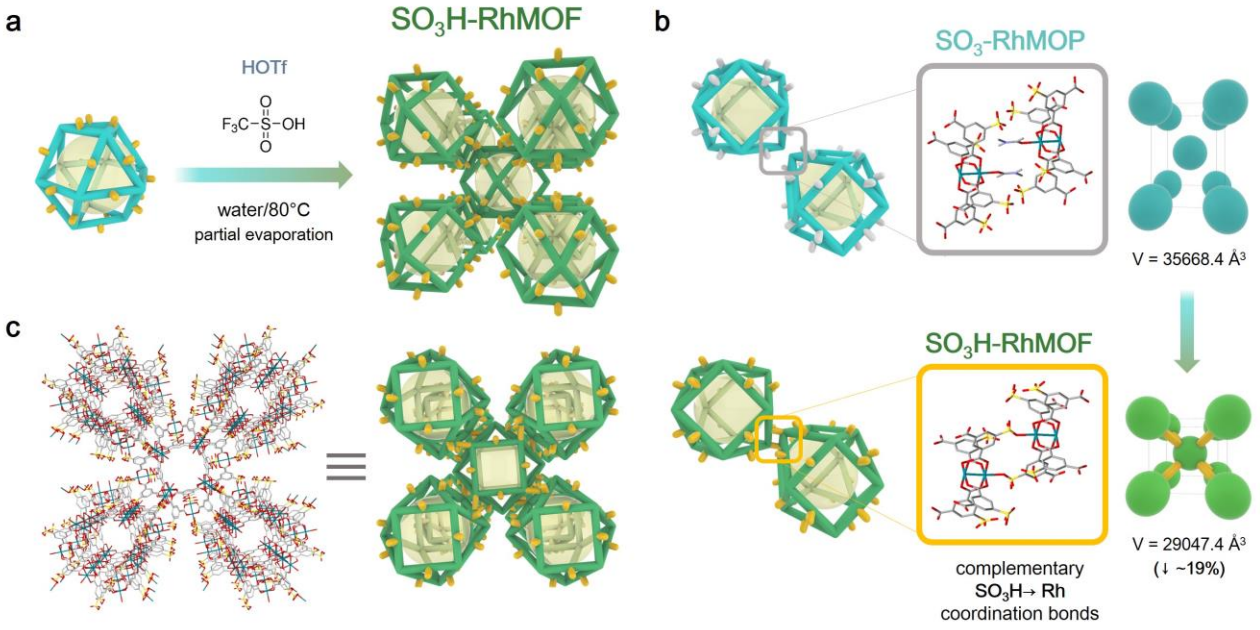

Figure 5. a) Schematic representation of the formation of from **SO_3H-RhMOP$_a$** in the presence of HOTf. b) Detailed view of the intercage space in **SO_3-RhMOP** (left) and **SO_3H-RhMOF** (right) crystal structures showing the connection between **SO_3H-RhMOP** cages trough complementary O → Rh bonds from sulfonic acid groups in **SO_3H-RhMOF** and the resulting contraction in the unit cell volume. c) View along the *c* axis of **SO_3H-RhMOF** crystals structure, showing the alignment of the cage pores.

resulting structure (Figure S17).[11, 12] In this case, the competition between DMSO solvent molecules and phenolic hydroxyl groups on the ligand dictates the degree of connectivity between the cages. Thus, the reduction of the DMSO concentration during crystallization involves the formation of networks with higher connectivity, 6-c and 4,6-c, whereas 4-c is formed when the DMSO concentration is increased. However, in all the cases the coordination of organic solvents (i.e. DMSO, MeOH, and DMF) exerts some steric hindrance around the metal site, limiting the formation of networks with higher connectivity. On the contrary, in the crystallization of **SO_3H-RhMOF** from **SO_3H-RhMOP$_a$**, the use of water as solvent involves minimum steric hindrance between solvated cages, allowing a denser packing to give an 8-c network. Thus, the high stability and solubility in water of **SO_3H-RhMOP$_a$** are crucial to achieve such type of connectivity. HOTf also plays a critical role in the formation of **SO_3H-RhMOF.** All the experiments without HOTf involving the evaporation of water solutions of **SO_3H-RhMOP$_a$**, with or without heating, yielded amorphous powders. The presence of HOTf not only guarantees a highly acid medium, favoring the formation of SO_3H-(bdc) groups, but also can aid crystallization by modulating the coordination equilibrium(Figure S18).[44] This effect was further investigated by using strong non-coordinating HBF_4 acid, which resulted in amorphous powders after water evaporation.

Despite the structural similarities between **SO_3-RhMOP** and **SO_3H-RhMOF**, the connection between the cages in **SO_3H-RhMOF** involves the reduction of the unit cell volume by ~19%, with a shortening of the unit cell along the [001] direction (~28%) and a smaller elongation along [100] and [010] directions (~6%). Correspondingly, the distance between the centers of the cages is shorter in **SO_3H-RhMOF** (26.613 Å) than in **SO_3-RhMOP** (29.342 Å). As in the case of **SO_3-RhMOP**, the alignment of the cages results in porous channels along the [001] direction (Figure 5c).

Bulk green amorphous **SO_3H-RhMOF$_a$** powder was obtained after washing and drying the as-synthesized **SO_3H-RhMOF** crystals. Comparison of TGA curves for **SO_3H-RhMOP$_a$** and **SO_3H-RhMOF$_a$** are much similar to each other, indicating a similar composition (Figure S19). **SO_3H-RhMOF$_a$** was found to be highly soluble in water, which involves its disassembly into discrete **SO_3H-RhMOP** (Figure S20) and confirms the reversible MOF-to-MOP transformation. Further, the high water solubility of **SO_3RhMOF** is in line with the fact that the evaporation of water was needed for the synthesis of crystals, since reactions in closed vials did not afford any precipitate. We attribute this behavior to the interaction between Rh atoms and water, which is favored against weaker sulfonic-Rh interaction.

Sorption Properties. The presence of solvent accessible voids in the crystal structures of synthesized materials, together with the high stability of Rh-based MOPs, prompted us to investigate their gas sorption properties. Note that powder X-ray diffraction (PXRD) patterns of the activated samples showed no peaks (Figure S21), pointing to the loss of long-range order upon solvent removal, which is common for carboxylate paddlewheel-based MOPs.

As depicted in Figure 6a, **SO_3-RhMOP$_a$** showed negligible N_2 uptake at 77 K, which can be attributed to the presence of $[Me_2NH_2]^+$ cations filling and/or blocking the pores. Contrariwise, **SO_3H-RhMOP$_a$** and **SO_3H-RhMOF$_a$** showed N_2 adsorption with typical type-I isotherms, characteristic of microporous materials, with BET surface areas of 313 and 500 $m^2\ g^{-1}$, respectively. We also estimated the pore size distribution (PSD) of these samples by non-local density functional theory (NLDFT). PSDs of **SO_3H-RhMOP$_a$** and **SO_3H-RhMOF$_a$** show maxima at 0.7 nm (Figure 6b), which correspond to the expected value for the cage cavity.[45] In addition, broader PSDs centered at *ca* 1.4 nm are also observed, which are assigned to the external voids generated upon packing (Figure S22). Although both solids are amorphous, in the case of **SO_3H-RhMOF$_a$** the contribution of this inter-cage pore is higher, being indicative of better retention of the inter-cage voids upon activation. Thus, the higher adsorption capacity observed for **SO_3H-RhMOF$_a$** can be ascribed to the higher contribution of the extrinsic porosity, as can be expected for an extended network in which cages are chemically bounded.

These results provide two main insights. First, adequate acid treatment (i.e. HOTf) is crucial for accessing to materials with permanent porosity. This is a consequence of the high acidity of sulfonic acid group, which involves the formation of $^-SO_3$-RhMOP-based salts under conventional synthetic conditions. Therefore, incorporated cations must be removed to favour gas uptake. Second, the extension of **SO_3H-RhMOP** discrete molecular cage to **SO_3H-RhMOF** 3D framework results in a significant improvement of the adsorption capacity. In this case, such effect can be attributed to the combination of the intrinsic porosity of the cage and the extrinsic porosity arising from its assembly into an ordered coordination network.[46]

CO_2 sorption measurements at 195 K were also conducted, showing the same trend (Figure 6c). Thus, **SO_3H-RhMOF$_a$** displayed the highest adsorption capacity at P/P_0~1.0 (132 $cm^3\ g^{-1}$), whereas **SO_3H-RhMOP$_a$** presented a value of 97 $cm^3\ g^{-1}$, which is much higher than that of **SO_3-RhMOP$_a$** (39 $cm^3\ g^{-1}$). The effect of processing **SO_3H-RhMOP** cage into **SO_3H-RhMOF** in the sorption behavior of was further confirmed. Thus, the N_2 (77 K) adsorption isotherm of the solid resulting from the solubilization and further precipitation of **SO_3H-RhMOF$_a$**, exhibited a lower BET surface area of 315 $m^2\ g^{-1}$, which is identical to the one displayed by **SO_3H-RhMOP$_a$** (Figure S23).

The presence of accessible hydrophilic -SO_3H groups in **SO_3H-RhMOP$_a$** and **SO_3H-RhMOF$_a$** motivated us to study their water sorption capacity. Figure 6d shows the water vapor isotherms at 298 K, revealing a similar behavior for both compounds with a very high water uptake. The water uptakes of **SO_3H-RhMOP$_a$** and **SO_3H-RhMOF$_a$** at 90% relative humidity (RH) were 412 and 376 $cm^3\ g^{-1}$, corresponding to 159 and 138 water molecules per cage, respectively. These values are higher than those of previously reported cages,[25,47-50] which can be attributed to the large amount of

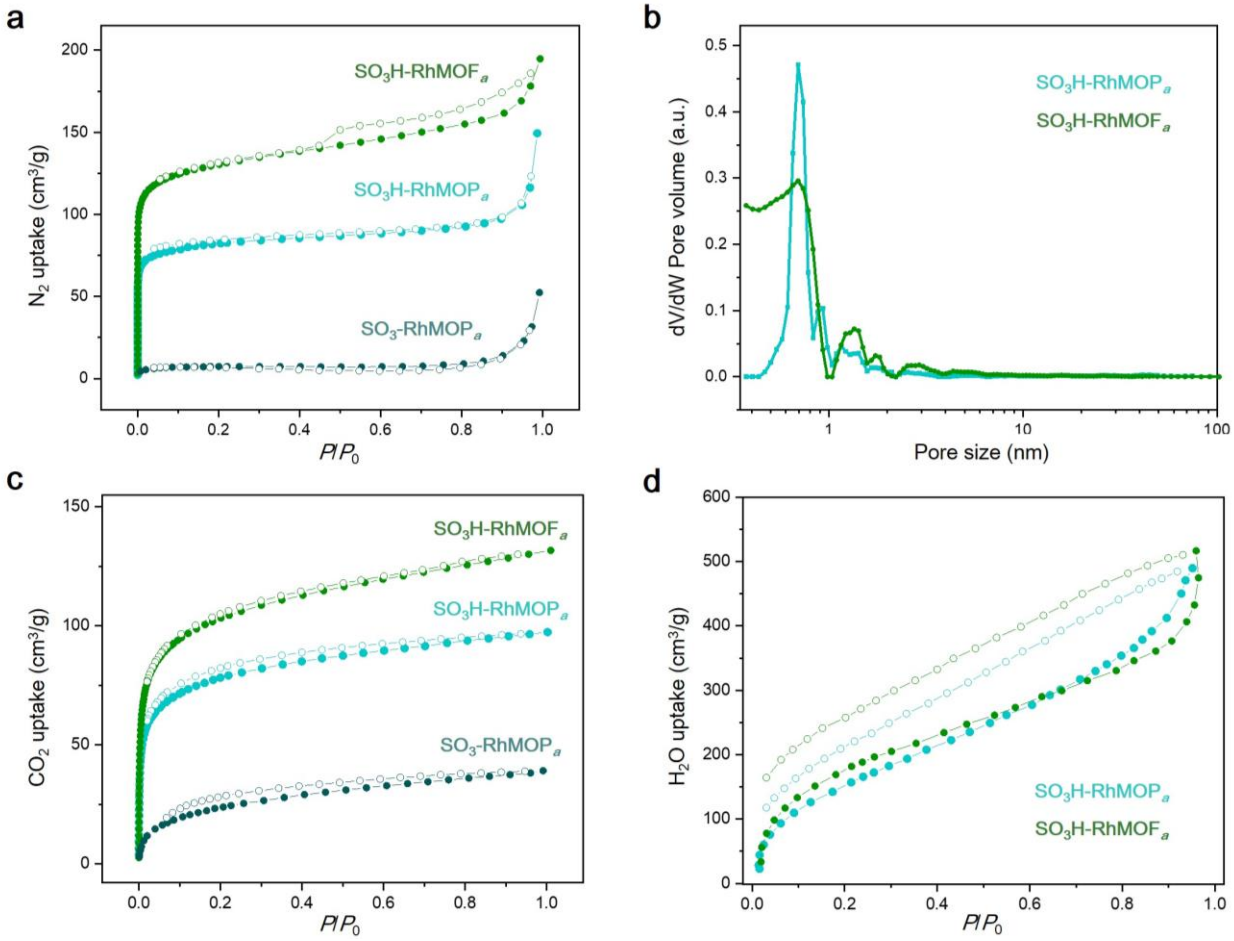

Figure 6. a) N_2 adsorption (filled circle) and desorption (open circle) at 77 K of **SO_3-RhMOP$_a$** (tale), **SO_3H-RhMOP$_a$** (turquoise) and **SO_3H-RhMOF$_a$** (green). b) Pore size distribution (PSD) of **SO_3H-RhMOP$_a$** (turquoise) and **SO_3H-RhMOF$_a$** (green) estimated from N2 isotherm by NLDFT on a slit pore model. c) CO2 adsorption (filled circle) and desorption (open circle) at 195 K of **SO_3-RhMOP$_a$** (tale), **SO_3H-RhMOP$_a$** (turquoise) and **SO_3H-RhMOF$_a$** (green). d) H2O adsorption (filled circle) and desorption (open circle) at 298 K of **SO_3H-RhMOP$_a$** (turquoise) and **SO_3H-RhMOF$_a$** (green).

highly hydrophilic -SO_3^-/-SO_3H groups on the MOP surface (24 per cage).

Proton conduction. It is known that compounds presenting a high concentration of sulfonic acid groups can show excellent proton conductivities.[51] The hydrophilic sulfonic groups can not only act as proton sources, but also can establish hydrogen bonds with neighboring water molecules, favoring the creation of efficient pathways for conduction. In our case, the high concentration of acidic sulfonic groups as well as the superior water vapor adsorption capacity exhibited by **SO_3H-RhMOP$_a$** and **SO_3H-RhMOF$_a$** drive us to investigate their potential as proton conducting materials. To this end, alternating-current (AC) impedance spectroscopy measurements were performed on pressed pellets of powder samples. The proton conductivity was estimated by fitting the semicircle of Nyquist plots. Preliminary test were conducted with **SO_3H-RhMOP$_a$**. At 25 °C and 60% RH, we found a moderate proton conductivity of 3.2×10^{-5} S cm^{-1}. We next kept the sample at 25 °C and increased humidity up to 90% RH, resulting in a higher conductivity value of 1.2×10^{-3} S cm^{-1} (Figure S24). The improvement of conductivity upon increasing humidity pointed out the relevant role of water in the proton transport. The effect of the temperature was also checked by measuring the conductivity at different temperatures (40-95 °C) while keeping RH constant at 90% (Figure 7a). **SO_3H-RhMOP$_a$** exhibited a continuous increment of conductivity upon heating, achieving a maximum value of 2.5 $\times 10^{-2}$ S cm^{-1} at 95°C (Figure 7c). Then, the proton conductivity of **SO_3H-RhMOF$_a$** at different temperatures (90% RH) was also measured, displaying a lower but still high conductivity value of 4.4×10^{-3} S cm^{-1} at 95°C (Figures 7b and 7c). The performance of the presented materials is in the range of previously reported high proton-conducting metal-organic compounds such MOFs and MOPs (>10^{-3} S cm^{-1}).[52] Particularly, compared to other conducting MOPs (Table S5), the conductivity exhibited by **SO_3H-RhMOP$_a$** is the highest for a MOP measured as compacted pellet of powder; and it is very close to the highest value obtained from a MOP single crystal measurement (5.8×10^{-2} S

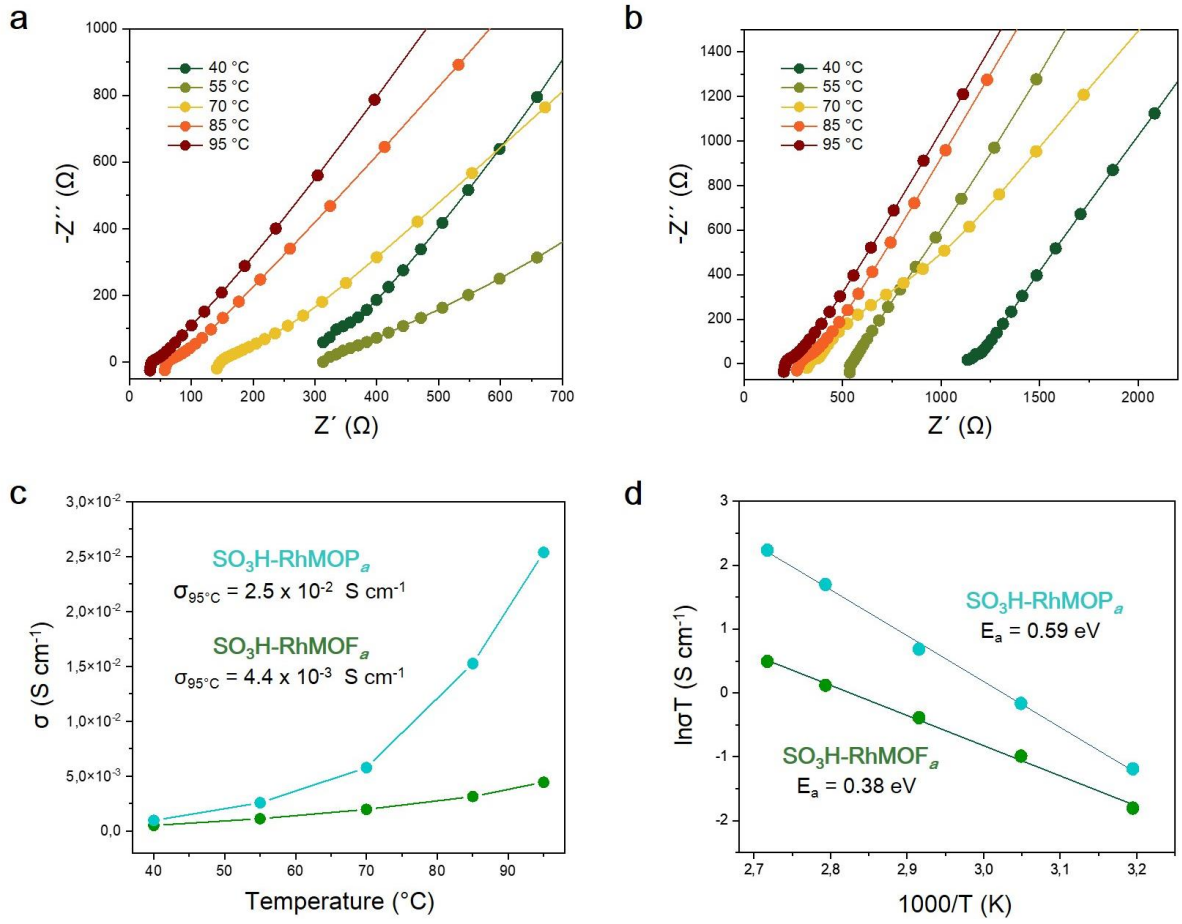

Figure 7. Temperature dependence of the Nyquist plot for **SO_3H-RhMOP*a*** (a) and **SO_3H-RhMOF*a*** (b) at RH = 90%. c) **SO_3H-RhMOP*a*** and **SO_3H-RhMOF*a*** proton conductivity variation versus temperature at RH = 90%. d) Arrhenius plots of **SO_3H-RhMOP*a*** and **SO_3H-RhMOF*a*** at RH = 90%.

cm^{-1}).[53] We attributed this high conductivity to the elevated number of sulfonic acid groups located at the outer surface of **SO_3H-RhMOP*a*** and the resulting high water adsorption capacity for both **SO_3H-RhMOP*a*** and **SO_3H-RhMOF*a***. Thus, previously reported sulfonate functionalized Zr-based MOP with six groups on its surface,[25] showed lower water adsorption capacity of ~240 cm^3 g^{-1} at 90% RH, exhibiting high conductivity (2.8×10^{-3} S cm^{-1}), but one order of magnitude lower than **SO_3H-RhMOP*a***. Likewise, the difference between **SO_3H-RhMOP*a*** and **SO_3H-RhMOF*a*** conductivities can be ascribed to the presence of coordinated sulfonic acid groups in **SO_3H-RhMOF*a***, which involves a smaller number of sulfonic acid groups available for conduction (16 per cage) compared to **SO_3H-RhMOP*a*** (24 per cage).

The activation energies E_a of proton conductivities from the Arrhenius plot (Figure 7d) were found to be E_a = 0.59 eV and E_a = 0.38 eV for **SO_3H-RhMOP*a*** and **SO_3H-RhMOF*a***, respectively. Despite these values are relatively high compared to typical hydrated proton conductors,[54] E_a values for **SO_3H-RhMOP*a*** and **SO_3H-RhMOF*a*** are lower to that found in other highly conducting MOPs (E_a > 0.65 mV).[50,53] The observed higher E_a for more conducting **SO_3H-RhMOP*a*** compared to less conducting **SO_3H-RhMOF*a***, with lower E_a, can be indicative of a complex conduction mechanism, in which both proton jumping through available sulfonic groups (Grotthuss mechanism) and direct transport with water molecules (vehicle mechanism) contribute to the proton conduction.[55]

CONCLUSIONS

Here, we present sulfonic acid-rich metal-organic polyhedra capable to undergo reversible MOP-to-MOF transformation *via* self-polymerization. The design of the cage relied on the combination of sulfonic acid groups that have moderate binding and high proton-donating capability, and [$Rh_2(COO)_4$] moiety with high chemical stability and available open metal sites. The resulting cage displayed high solubility and stability in water over a wide range of pH, which allowed to modify its acidic capacity through post-synthetic acid treatment. The former is important when thinking in the use of MOPs in biomedical applications, since the cage should be soluble in most physiological pH values, while the latter opens the door to its further use as water-soluble acid catalyst. Likewise, complementary coordination bonds between external sulfonic acid groups and Rh_2 units led to the formation of a highly connected 3D MOF structure. The effect of the MOP-to-MOF processing was reflected in their different adsorption and

conducting properties: MOF network showed higher gas adsorption capacity while isolated MOP cage present superior conducting properties. The chemistry reported here points towards the use of stable but coordinatively unsaturated metallic nodes in combination with external acidic functional groups as a design basis for MOPs. The application of this principle to another acidic functional groups/open metal sites or different cage geometries is expected to provide pH-independent water-soluble cages, molecular acid catalysts, unusual MOP-based MOF architectures, and high proton-conducting materials.

ASSOCIATED CONTENT

Supporting Information.

Full experimental procedures, PXRD, SC-XRD, UV–vis, FT-IR, ^{1}H NMR, thermogravimetric analysis, elemental analysis, and sorption data.

Supporting movie 1

X-ray crystallographic data in CIF format for **SO3-RhMOP(Me2NH)** (CCDC 2191318)

X-ray crystallographic data in CIF format for **SO3-RhMOP** (CCDC 2191319)

X-ray crystallographic data in CIF format for **SO3H-RhMOF** (CCDC 2191317)

This material is available free of charge via the Internet at http://pubs.acs.org.

AUTHOR INFORMATION

Corresponding Authors

Javier Troyano – Institute for Integrated Cell-Material Sciences (WPI-iCeMS), Kyoto University, iCeMS Research Building, Yoshida, Sakyo-ku, Kyoto 606-8501, Japan and Departamento de Química Inorgánica, Universidad Autónoma de Madrid, 28049 Madrid, Spain; Email: javier.troyano@uam.es

Shuhei Furukawa – Institute for Integrated Cell-Material Sciences (WPI-iCeMS), Kyoto University, Sakyo-ku, Kyoto 606-8501, Japan; Email: shuhei.furukawa@icems.kyoto-u.ac.jp

Notes

The authors declare no competing financial interest

ACKNOWLEDGMENT

J.T. is grateful to the Japan Society for the Promotion of Science (JSPS) for Post-Doctoral Fellowship. This study is supported by JSPS KAKENHI Grant Number 21K18192 (Challenging Research (Pioneering)) for S. F. The authors acknowledge the iCeMS Analysis Center for access to analytical facilities. The authors also thank Ms. Nanae Shimanaka for assistance in the conductivity measurements.

REFERENCES

(1) Tranchemontagne, D. J.; Ni, Z.; O'Keeffe, M.; Yaghi, O. M. Reticular Chemistry of Metal–Organic Polyhedra. *Angew. Chem., Int. Ed.* **2008**, 47, 5136.

(2) Guillerm, V.; Kim, D.; Eubank, J. F.; Luebke, R.; Liu, X.; Adil, K.; Lah, M. S.; Eddaoudi, M. A supermolecular building approach for the design and construction of metal–organic frameworks. *Chem. Soc. Rev.* **2014**, 43, 6141.

(3) Percástegui, E. G.; Ronson, T. K.; Nitschke, J. R. Design and Applications of Water-Soluble Coordination Cages. *Chem. Rev.* **2020**, 120, 13480.

(4) Zhang, D.; Ronson, T. K.; Zou, Y.-Q.; Nitschke, J. R. Metal–organic cages for molecular separations. *Nat. Rev. Chem.* **2021**, 5, 168.

(5) Gosselin, A. J.; Rowland, C. A.; Bloch, E. D. Permanently Microporous Metal–Organic Polyhedra. *Chem. Rev.* **2020**, 120, 8987.

(6) Lee, S.; Jeong, H.; Nam, D.; Lah, M. S.; Choe, W. The rise of metal–organic polyhedra.*Chem. Soc. Rev.* **2021**, 50, 528.

(7) Nam, D.; Kim, J.; Hwang, E.; Nam, J.; Jeong, H.; Kwon, T.-H.; Choe, W. Multivariate porous platform based on metal-organic polyhedra with controllable functionality assembly. *Matter* **2021**, 4, 2460.

(8) Albalad, J.; Hernández-López, L.; Carné-Sánchez, A.; Maspoch, D. Surface chemistry of metal–organic polyhedra. *Chem. Commun.* **2022**, 58, 2443.

(9) Lal, G.; Lee, S. J.; Spasyuk, D. M.; Shimizu, G. K. H. Amphiphile-like self assembly of metal organic polyhedra having both polar and non-polar groups. *Chem. Commun.* **2018**, 54, 1722.

(10) Albalad, J.; Carné-Sánchez, A.; Grancha, T.; Hernández-López, L.; Maspoch, D. Protection strategies for directionally-controlled synthesis of previously inaccessible metal–organic polyhedra (MOPs): the cases of carboxylate- and amino-functionalised Rh(II)-MOPs. *Chem. Commun.* **2019**, 55, 12785.

(11) Mollick, S.; Fajal, S.; Mukherjee, S.; Ghosh, S. K. Stabilizing Metal–Organic Polyhedra (MOP): Issues and Strategies. *Chem. Asian J.* **2019**, 14, 3096.

(12) Grancha, T.; Carné-Sánchez, A.; Hernández-López, L.; Alba-lad, J.; Imaz, I.; Juanhuix, J.; Maspoch, D. Phase Transfer of Rhodium(II)-Based Metal–Organic Polyhedra Bearing Coordinatively Bound Cargo Enables Molecular Separation. *JACS* **2019**, 141, 18349.

(13) Kawano, R.; Horike, N.; Hijikata, Y.; Kondo, M.; Carné-Sánchez, A.; Larpent, P.; Ikemura, S.; Osaki, T.; Kamiya, K.; Kitagawa, S.; Takeuchi, S.; Furukawa, S. Metal-Organic Cuboctahedra for Synthetic Ion Channels with Multiple Conductance States. *Chem* **2017**, 2, 393.

(14) Khobotov-Bakishev, A.; Hernández-López, L.; von Baeckmann, C.; Albalad, J.; Carné-Sánchez, A.; Maspoch, D. Metal–Organic Polyhedra as Building Blocks for Porous Extended Networks. *Adv. Sci.* **2022**, 9, 2104753.

(15) Sánchez-González, E.; Tsang, M. Y.; Troyano, J.; Craig, G. A.; Furukawa, S. Assembling metal–organic cages as porous materials. *Chem. Soc. Rev.* **2022**, 51, 4876.

(16) Hosono, N.; Kitagawa, S. Modular Design of Porous Soft Materials via Self-Organization of Metal–Organic Cages *Acc. Chem. Res.* **2018**, 51, 2437.

(17) Kim, J.; Choe, W. Topology-guided roadmap for reticular chemistry of metal-organic polyhedra. *Chem* **2022**, 8, 617.

(18) Li, J.-R.; Timmons, D. J.; Zhou, H.-C. Interconversion between Molecular Polyhedra and Metal–Organic Frameworks. *JACS* **2009**, 131, 6368.

(19) Chun, H.; Jung, H.; Seo, J. Isoreticular Metal-Organic Polyhedral Networks Based on 5-Connecting Paddlewheel Motifs. *Inorg. Chem.* **2009**, 48, 2043.

(20) Nam, D.; Huh, J.; Lee, J.; Kwak, J. H.; Jeong, H. Y.; Choi, K.; Choe, W. Cross-linking Zr-based metal–organic polyhedra via postsynthetic polymerization. *Chem. Sci.* **2017**, 8, 7765.

(21) Grancha, T.; Carné-Sánchez, A.; Zarekarizi, F.; Hernández-López, L.; Albalad, J.; Khobotov, A.; Guillerm, V.; Morsali, A.; Juan-huix, J.; Gándara, F.; Imaz, I.; Maspoch, D. Synthesis of Polycarboxylate Rhodium(II) Metal–Organic Polyhedra (MOPs) and their use as Building Blocks for Highly Connected Metal–Organic Frameworks (MOFs).*Angew. Chem., Int. Ed.* **2021**, 60, 5729.

(22) McManus, G. J.; Wang, Z.; Zaworotko, M. J. Suprasupermolecular Chemistry: Infinite Networks from Nanoscale Metal–Organic Building Blocks. *Cryst. Growth Des.* **2004**, 4, 11.

(23) Niu, Z.; Fang, S.; Liu, X.; Ma, J.-G.; Ma, S.; Cheng, P. Coordination-Driven Polymerization of Supramolecular Nanocages. *JACS* **2015**, 137, 14873.

(24) Niu, Z.; Wang, L.; Fang, S.; Lan, P. C.; Aguila, B.; Perman, J.; Ma, J.-G.; Cheng, P.; Li, X.; Ma, S. Solvent-assisted coordination driven assembly of a supramolecular architecture featuring two types of connectivity from discrete nanocages. *Chem. Sci.* **2019**, 10, 6661.

(25) Xing, W.-H.; Li, H.-Y.; Dong, X.-Y.; Zang, S.-Q. Robust multifunctional Zr-based metal–organic polyhedra for high proton conductivity and selective CO2 capture. *J. Mater. Chem. A* **2018**, 6, 7724.

(26) Mal, P.; Schultz, D.; Beyeh, K.; Rissanen, K.; Nitschke, J. R. An Unlockable–Relockable Iron Cage by Subcomponent Self-Assembly. *Angew. Chem., Int. Ed.* **2008**, 47, 8297.

(27) Ma, L.; Haynes, C. J. E.; Grommet, A. B.; Walczak, A.; Parkins, C. C.; Doherty, C. M.; Longley, L.; Tron, A.; Stefankiewicz, A. R.; Bennett, T. D.; Nitschke, J. R. Coordination cages as permanently porous ionic liquids. *Nat. Chem.* **2020**, 12, 270.

(28) Li, J.-R.; Zhou, H.-C. Bridging-ligand-substitution strategy for the preparation of metal–organic polyhedra. *Nat. Chem.* **2010**, 2, 893.

(29) Tan, Y.-X.; He, Y.-P.; Zhang, J. Pore partition effect on gas sorption properties of an anionic metal–organic framework with exposed Cu^{2+} coordination sites. *Chem. Commun.* **2011**, 47, 10647.

(30) Warzecha, E.; Berto, T. C.; Wilkinson, C. C.; Berry, J. F. Rhodium Rainbow: A Colorful Laboratory Experiment Highlighting Ligand Field Effects of Dirhodium Tetraacetate. *J. Chem. Educ.* **2019**, 96, 571.

(31) Guthrie, J. P. Hydrolysis of esters of oxy acids: pKa values for strong acids; Brønsted relationship for attack of water at methyl; free energies of hydrolysis of esters of oxy acids; and a linear relationship between free energy of hydrolysis and pKa holding over a range of 20 pK units.*Can. J. Chem.* **1978**, 56, 2342.

(32) Vetromile, C. M.; Lozano, A.; Feola, S.; Larsen, R. W. *Inorg. Chim. Acta* **2011**, 378, 36.

(33) Shimizu, G. K. H.; Vaidhyanathan, R.; Taylor, J. M. Phosphonate and sulfonate metal organic frameworks. *Chem. Soc. Rev.* **2009**, 38, 1430.

(34) Côté, A. P.; Shimizu, G. K. H. The supramolecular chemistry of the sulfonate group in extended solids. *Coord. Chem. Rev.* **2003**, 245, 49.

(35) Cai, J. Structural chemistry and properties of metal arenesulfonates. *Coord. Chem. Rev.* **2004**, 248, 1061.

(36) Videnova-Adrabinska, V. Coordination and supramolecular network entanglements of organodisulfonates *Coord. Chem. Rev.* **2007**, 251, 1987.

(37) Wang, Z.; Aoyama, T.; Sánchez-González, E.; Inose, T.; Urayama, K.; Furukawa, S. Control of Extrinsic Porosities in Linked Metal–Organic Polyhedra Gels by Imparting Coordination-Driven Self-Assembly with Electrostatic Repulsion. *ACS Appl. Mater. Interfaces* **2022**, 14, 23660.

(38) Carné-Sánchez, A.; Albalad, J.; Grancha, T.; Imaz, I.; Juanhuix, J.; Larpent, P.; Furukawa, S.; Maspoch, D. Postsynthetic Covalent and Coordination Functionalization of Rhodium(II)-Based Metal–Organic Polyhedra. *JACS* **2019**, 141, 4094.

(39) Furukawa, S.; Horike, N.; Kondo, M.; Hijikata, Y.; Carné-Sánchez, A.; Larpent, P.; Louvain, N.; Diring, S.; Sato, H.; Matsuda, R.; Kawano, R.; Kitagawa, S. Rhodium–Organic Cuboctahedra as Porous Solids with Strong Binding Sites. *Inorg. Chem.* **2016**, 55, 10843.

(40) Carné-Sánchez, A.; Craig, G. A.; Larpent, P.; Hirose, T.; Higuchi, M.; Kitagawa, S.; Matsuda, K.; Urayama, K.; Furukawa, S. Self-assembly of metal–organic polyhedra into supramolecular polymers with intrinsic microporosity. *Nat. Commun.* **2018**, 9, 2506.

(41) Nückel, S.; Burger, P. Transition Metal Complexes with Sterically Demanding Ligands, 3.1 Synthetic Access to Square-Planar Terdentate Pyridine–Diimine Rhodium(I) and Iridium(I) Methyl Complexes: Successful Detour via Reactive Triflate and Methoxide Complexes. *Organometallics* **2001**, 20, 4345.

(42) Dias, E. L.; Brookhart, M.; White, P. S. Stable, Cationic Alkyl–Olefin Complexes of Ruthenium(II) and Rhodium(III): Effects of Ligand Geometry upon Olefin Insertion/Alkyl Migration. *Organometallics* **2000**, 19, 4995.

(43) Rowsell, B. D.; McDonald, R.; Cowie, M. Bridging Methylene to Bridging Acyl Conversion in Heterobinuclear Rh/Ru Complexes: Models for Adjacent-Metal Involvement in Bimetallic Catalysts. *Organometallics* **2004**, 23, 3873.

(44) Tsuruoka, T.; Furukawa, S.; Takashima, Y.; Yoshida, K.; Iso-da, S.; Kitagawa, S. Nanoporous Nanorods Fabricated by Coordination Modulation and Oriented Attachment Growth. *Angew. Chem., Int. Ed.* **2009**, 48, 4739.

(45) Wang, Z.; Villa Santos, C.; Legrand, A.; Haase, F.; Hara, Y.; Kanamori, K.; Aoyama, T.; Urayama, K.; Doherty, C. M.; Smales, G. J.; Pauw, B. R.; Colón, Y. J.; Furukawa, S. Multiscale structural control of linked metal–organic polyhedra gel by aging-induced linkage-reorganization. *Chem. Sci.* **2021**, 12, 12556.

(46) Sánchez-González, E.; Tsang, M. Y.; Troyano, J.; Craig, G. A.; Furukawa, S. Assembling metal–organic cages as porous materials. *Chem. Soc. Rev.* **2022**.

(47) Samanta, D.; Chowdhury, A.; Mukherjee, P. S. Covalent Postassembly Modification and Water Adsorption of Pd3 Self-Assembled Trinuclear Barrels. *Inorg. Chem.* **2016**, 55, 1562.

(48) Liu, G.; Di Yuan, Y.; Wang, J.; Cheng, Y.; Peh, S. B.; Wang, Y.; Qian, Y.; Dong, J.; Yuan, D.; Zhao, D. Process-Tracing Study on the Postassembly Modification of Highly Stable Zirconium Metal–Organic Cages. *JACS* **2018**, 140, 6231.

(49) Samanta, D.; Mukherjee, P. S. Component Selection in the Self-Assembly of Palladium(II) Nanocages and Cage-to-Cage Transformations. *Eur. J. Chem.* **2014**, 20, 12483.

(50) Saha, R.; Samanta, D.; Bhattacharyya, A. J.; Mukherjee, P. S. Stepwise Construction of Self-Assembled Heterometallic Cages Showing High Proton Conductivity. *Eur. J. Chem.* **2017**, 23, 8980.

(51) Liu, R.-l.; Wang, D.-Y.; Shi, J.-R.; Li, G. Proton conductive metal sulfonate frameworks. *Coord. Chem. Rev.* **2021**, 431, 213747.

(52) Lim, D.-W.; Kitagawa, H. Rational strategies for proton-conductive metal–organic frameworks. *Chem. Soc. Rev.* **2021**, 50, 6349.

(53) Zhai, Q.-G.; Mao, C.; Zhao, X.; Lin, Q.; Bu, F.; Chen, X.; Bu, X.; Feng, P. Cooperative Crystallization of Heterometallic Indium–Chromium Metal–Organic Polyhedra and Their Fast Proton Conductivity. *Angew. Chem., Int. Ed.* **2015**, 54, 7886.

(54) Sadakiyo, M.; Yamada, T.; Kitagawa, H. Hydrated Proton-Conductive Metal–Organic Frameworks. *ChemPlusChem* **2016**, 81, 691.

(55) Sadakiyo, M.; Yamada, T.; Kitagawa, H. Proton Conductivity Control by Ion Substitution in a Highly Proton-Conductive Metal–Organic Framework. *JACS* **2014**, 136, 13166.